

Kondo versus Fano in superconducting artificial high- T_c heterostructures

Gaetano Campi^{1,2*} Gennady Logvenov³ Sergio Caprara^{4*} Antonio Valletta⁵ Antonio Bianconi^{1,2*}

¹*Institute of Crystallography, Italian National Research Council, IC-CNR, Via Salaria Km 29.300, 00015 Roma, Italy email: gaetano.campi@ic.cnr.it*

²*Rome International Center for Materials Science Superstripes RICMASS, Via dei Sabelli 119A, 00185 Roma, Italy; email antonio.bianconi@ricmass.eu,*

³*Max Planck Institute for Solid State Research, Heisenbergstraße 1, 70569 Stuttgart, Germany; email: g.logvenov@fkf.mpg.de,*

⁴*Department of Physics, Sapienza Università di Roma, P.le Aldo Moro, 5, 00185 Roma email: Italy email. sergio.caprara@uniroma1.it,*

⁵*Institute for Microelectronics and Microsystems, Italian National Research Council IMM-CNR, Via del Fosso del Cavaliere, 100, 00133 Roma, Italy. email: antonio.valletta@cnr.it*

*Authors to whom correspondence should be addressed: gaetano.campi@ic.cnr.it; antonio.bianconi@ricmass.eu; sergio.caprara@uniroma1.it; g.logvenov@fkf.mpg.de

Abstract

Recently, the quest for high- T_c superconductivity has evolved from the trial-and-error methodology to the growth of nanostructured artificial high- T_c superlattices (AHTS) with tailor-made superconducting functional properties by quantum design. Superlattices are composed of nanoscale superconducting units of modulation doped Mott insulator La_2CuO_4 with thickness L intercalated by metallic overdoped $\text{La}_{1.55}\text{Sr}_{0.45}\text{CuO}_4$ and period d . Quantum design based on the multi-gap Bogoliubov theory including spin-orbit coupling (SOC). has been employed for prediction of the amplification of the critical temperature as a function of the conformational parameter L/d . At the top of the superconducting dome, at the *magic* ratio $L/d=2/3$, the heterostructures are tuned at the Fano-Feshbach resonance and the normal phase exhibits the Planckian T -linear resistivity. Here, we report experimental evidence that the Kondo proximity effect competes with the Fano-Feshbach resonance suppressing T_c on both sides of the superconducting dome. The Kondo proximity effect is expected in electrical resistance of AHTS nanoscale heterostructures following a Kondo universal scaling obtained by numerical renormalization group theory. We show the vanishing Kondo temperature T_K and Kondo scattering amplitude R_{0K} at $L/d=2/3$, while T_K and R_{0K} increase on the underdoped ($L/d>2/3$) and overdoped ($L/d<2/3$) side of the superconducting dome.

Introduction

It is known that high- T_c cuprate superconductors can now be engineered by relying on the quantum design of nanoscale artificial high- T_c superlattices (AHTS) of quantum wells [1-3] that capture key features of natural chemically doped cuprates. The growth of these novel nanoscale non-conventional heterostructures has been guided by quantum material design of an artificially modulation-doped [4] correlated electron gas. This design relies on the predictions of the Bianconi-Perali-Valletta (BPV) theory [5-8] describing the amplification of the critical temperature driven by Fano-Feshbach shape

resonance [9-12] in two-gap superconductors in the presence of spin-orbit coupling (SOC) at the interfaces in nanostructured materials (NsM) exhibiting quantum size effects.

The three-dimensional AHTS heterostructures are formed by superconductor layers (S) of a stoichiometric modulation-doped Mott insulator La_2CuO_4 (LCO), intercalated with potential barriers of normal metal (N) made of chemically overdoped non-superconducting $\text{La}_{1.55}\text{Sr}_{0.45}\text{CuO}_4$ (LSCO) with ten repeats of period variable in the nanoscale range $2.97 < d < 5.28$ nm. The N units plays the role of charge reservoirs and transfer the interface space charge into the superconducting doped Mott insulator units of thickness L. The internal interface electric field at the SNS junctions induces Rashba SOC in the superconducting interface space charge in the S layers which is split into two electronic components by quantum size effects: the lowest subband shows a large cylindrical Fermi surface with *high* Fermi velocity, while the upper subband, exhibits a *low* Fermi velocity and an unconventional extended van Hove singularity generated by SOC at the interface.

Here, we show that at the top of superconducting dome driven by Fano-Feshbach shape resonance the normal phase shows the Planckian T-linear resistivity [13] which competes with Kondo scattering [14-28], resulting in the suppression of T_c on the two sides of the dome. The key result of this work, carried out above the top of the superconducting dome, i.e., in the range $50 \text{ K} < T < 270 \text{ K}$, is the compelling evidence that the temperature dependent sheet resistance of various AHTS in the normal phase evolves as the ratio L/d changes.

It is known that the Kondo proximity effect appears in nanoscale heterostructures of interest in this work. [15]. While the large charge correlation gap due to the local Coulomb repulsion U prohibits tunneling of electrons from the metal into a Mott insulator, the resonant spin flip scattering opens a new channel for tunneling, in this manner the metal ‘eats’ itself layer by layer into the Mott insulator. This is known as *Kondo proximity effect*, which promotes the formation of metallic interface space charge within the Mott insulator. A peculiar temperature dependence of the Kondo resistivity has been predicted [16] and it was observed in two-component electronic systems, like, e.g., $\text{SrTiO}_3/\text{LaTiO}_3/\text{SrTiO}_3$ heterostructures [17].

Evidence of the Kondo scattering of itinerant electrons by localized electrons has been reported in systems with logarithmic van Hove singularities [18], heavy fermions [19], vanadium dichalcogenides [20], nickelates [21], PrO epitaxial thin films [22], twisted bilayer graphene [23], cuprates [24,25], including Rashba SOC [26]. In our AHTS the superconducting transition temperature is amplified by Fano-Feshbach shape resonance between two superconducting gaps tuned by quantum size effects in the doped Mott insulator nanoscale layers of thickness L due to resonant scattering between closed and open scattering channels. The Fano-Feshbach shape

resonance in nanoscale heterostructures has been shown to compete [27] and coexist [28,29] with the Kondo scattering effect.

Results

In this work we report experimental evidence of the competition between the Kondo scattering and the Fano-Feshbach shape resonance in AHTS by tuning the chemical potential making quantum superlattices with variable L/d . While the electronic structure of the 2D electron gas at cuprate oxide interfaces with the associated interlayer phase separation has attracted high interest [30,31] we focus on quantum size effects due to confinement of the interphase correlated electron gas in the nanoscale [1]. We have first synthesized AHTS made of quantum wells with period $2.97 \text{ nm} < d < 5.28 \text{ nm}$, tuned at the magic resonant geometry, where pure Mott insulators LCO layers of thickness L , free of chemical substitutions, are intercalated with metallic LSCO layers of thickness W , so that $L/d = 2/3$, where $d = L + W$. These superlattices exhibit T-linear resistivity in the metallic phase from 50 K to 270 K. By changing the conformational geometry parameter away from the shape resonance, in the range $0.3 < L/d < 0.9$, we observe a Kondo-like temperature dependence in the resistivity, with the Kondo temperature T_K being minimum at $L/d = 2/3$, where the superconducting critical temperature is maximum and the amplitude of the Kondo effect in the resistivity, R_{0K} , is minimum.

Therefore, we report compelling evidence that the Kondo scattering competes with the Fano-Feshbach shape resonance.

Nanoscale LSCO/LCO superlattices of alternating overdoped LSCO layers and undoped LCO layers have been grown on a LaSrAlO_4 substrate using molecular beam epitaxy (MBE). These superlattices form a 2D electron gas (2DEG) at the interface space charge and exhibit 2D high- T_c superconductivity. The overall superlattice structure has a periodicity represented by the parameter d , as shown in Figure 1a.

Our experimental approach involves the manipulation of the 2DEG interface space charge layer, which extends approximately 2.6 nm into the LCO layer from the LSCO/LCO interface. This layer experiences quantum confinement between two LSCO potential barriers, whose width is denoted as W , within the superlattice. As a result, two artificial subbands emerge, allowing us to modulate their energy splitting or the transparency of the potential barrier by adjusting the thickness ratio L/d . **Figure 1a** depicts a typical LSCO/LCO superlattice with a period of $d = 3.96 \text{ nm}$. In this arrangement, the heterostructure consists of five LCO layers (ML), with thickness $L = 2.64 \text{ nm}$, while the LSCO layer has a thickness of half ML, $W = 1.32 \text{ nm}$. The superconducting critical temperature T_c , as a function of L/d assumes a dome shape where, at $L/d = 2/3$, the Fano-Feshbach shape resonance prevails and T_c reaches its maximum values, as shown in Figure 1b.

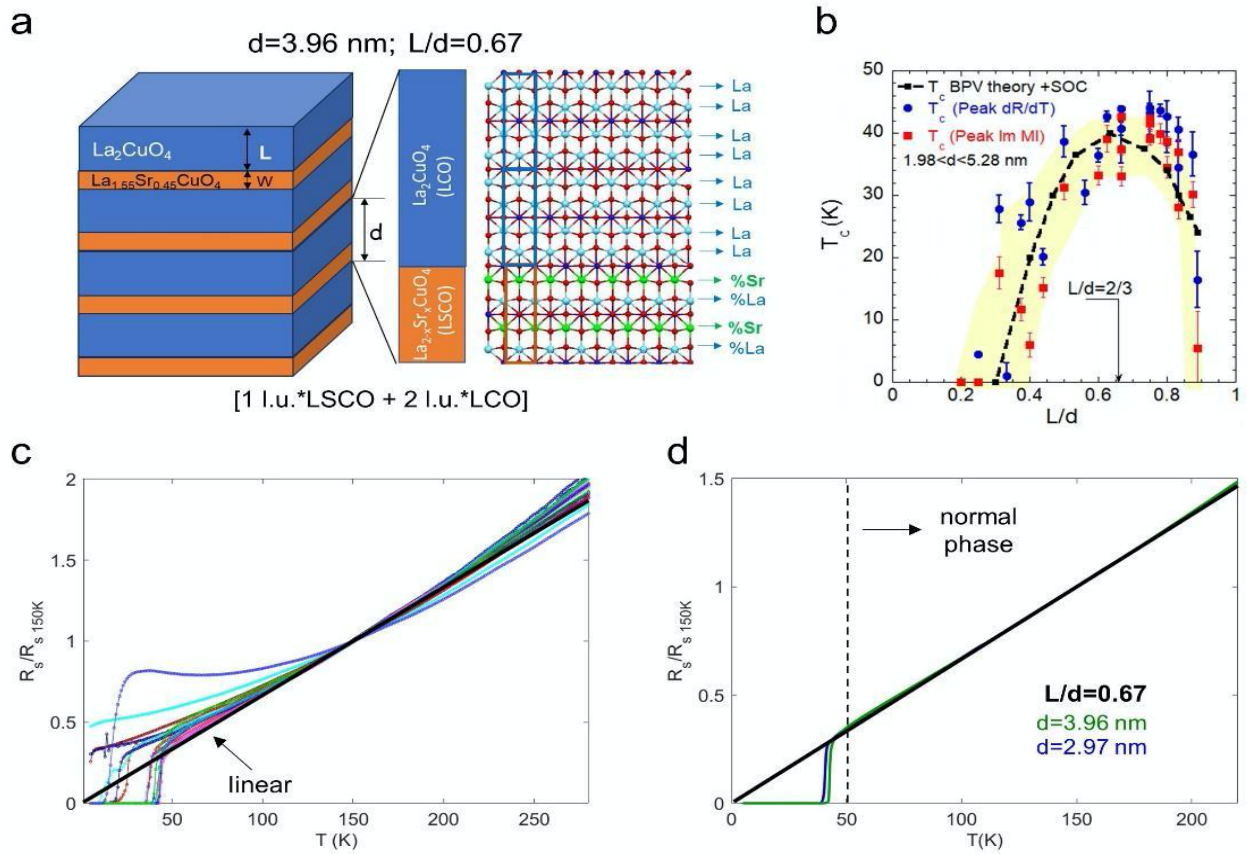


Figure 1. (a) Pictorial view of a practical realization of the nanoscale AHTS superlattice of quantum wells made of four monolayers ML ($L = 2.64$ nm) of undoped La_2CuO_4 (LCO), electronically doped by the interface space charge, which are intercalated by normal metal units made of two monolayers ML ($W = 1.32$ nm) of $\text{La}_{1.55}\text{Sr}_{0.45}\text{CuO}_4$ (LSCO) forming a superlattice with a period of $d = L + W = 3.96$ nm and with conformational parameter $L/d = 2/3$ giving the optimum critical temperature. (b) The superconductivity dome of the critical temperature T_c as a function of L/d in the range of $0.25 < L/d < 0.9$. The dashed line represents the predictions by the BPV theory at a Fano-Feshbach shape resonance for the superlattice of quantum wells. We show the T_c determined as maximum of a derivative of the sheet resistance (blue circles) and maximum of the imaginary part of the mutual inductance (red squares). (c) Sheet resistance as a function of temperature of several LSCO/LCO superlattices where it is normalized at $R_s|_{150\text{K}}$ which is the resistance measured at 150 K. The samples show the maximum $T_c \approx 43$ K around $L/d = 2/3$ corresponding to a critical temperature in the optimum doped LSCO. We draw a linear behavior (tick black line) observing how the samples with maximum T_c , with $L/d=2/3$, approach this linear resistivity regime. (d) shows the normalized sheet resistance as a function of temperature of two LSCO/LCO superlattices with $L/d = 2/3$ and different periods $d = 3.96$ nm and 2.97 nm showing T-linear resistivity in the temperature range $50 \text{ K} < T < 270 \text{ K}$.

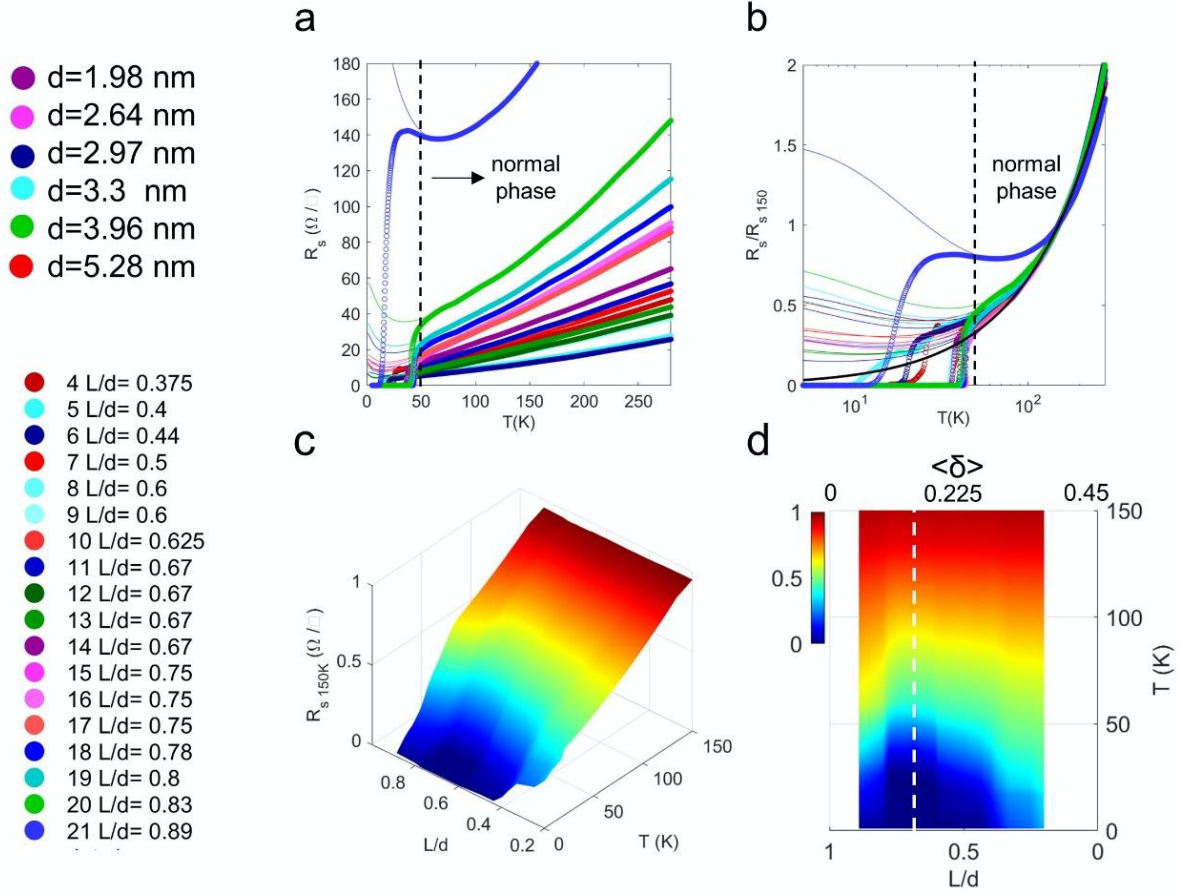


Figure 2. (a) (open circles) Sheet resistance as a function of temperature of 18 superlattices samples with different d and L values indicated in the list on the left. The different d -values correspond to the different colors indicated. (b) Normalized sheet resistance as a function of temperature alongside the modeled lines through Eq. 1. We show both the (left panel) linear and the (right panel) logarithmic evolution with temperature. (c) Color maps of normalized sheet resistance as a function of temperature, the geometrical parameter L/d . In panel (d) we show the correspondence between L/d and $\langle \delta \rangle = 0.45 (1-L/d)$. The white dashed line indicates $L/d = 2/3$ value.

We measured the temperature dependence of the resistance in eighteen LSCO/LCO superlattices with varying values of d , L , and W . The changes in resistivity with temperature, as shown in **Figure 1c**, display curves that both approach and deviate from a linear trend (thick black line). The resistances that most closely follow a linear pattern are reported in **Figure 1d**, where we present the resistance of two significant samples. These samples have the same L/d parameter ($L/d = 2/3$) but exhibit different d -periodicities. At this L/d value, where the superlattices approach the maximum T_C , the FFBR prevails, and a T -linear resistivity is observed in the normal phase.

To investigate the interplay of Fano resonance and Kondo scattering, away from the top of the superconducting dome, we consider here the sheet resistance as a function of temperature and L/d in the measured eighteen LCO/LSCO superlattices listed in Figure 2. These samples have been

classified by different d -values, corresponding to different colors and different L/d values. The sheet resistance of all eighteen superlattices, as a function of temperature, are shown in **Figure 2a**, while **Figure 2c** depicts the normalized sheet resistance in units of $R(T=150K)$, in semilogarithmic scale. All $R(T)$ curves have been fitted by using the generalized Kondo equation [16,17]:

$$\frac{R(T)}{R(T=150K)} = r_0 + \frac{T}{150} + AT^2 + BT^5 + \frac{R_{0K}}{\left\{1 + \left(\frac{1}{2^{\frac{1}{s}} - 1}\right) \left(\frac{T}{T_K}\right)^2\right\}^s} \quad (1)$$

for experimental $R(T)$ values measured at $T > 50K$. The *Kondo temperature* T_K represents a characteristic temperature below which the coupling between the impurity and conduction electrons leads to the screening of the impurity spin. R_{0K} is the amplitude of the Kondo-like contribution, while r_0 is the residual contribution at $T=0$, that represents the baseline resistivity of the material in the absence of Kondo physics including contributions such as impurities and lattice defects. The term AT^2 accounts for electron-electron scattering, while BT^5 represents phonon scattering. Both AT^2 and BT^5 terms are non-Kondo contributions. The best fitted curves are represented by continuous lines. The three different representations (Figure 2, panels **a**, and **b**) of the sheet resistance well visualize the fact that the resistivity decreases as the temperature is lowered, reaching a minimum. At even lower temperatures, the electrical resistivity of the system increases (logarithmically, in the original perturbative Kondo treatment, or as a power-law, beyond perturbation theory). We observe how the behavior of the resistance deviates from linearity as the L/d value moves away from $2/3$, where the Fano resonance prevails. A phase diagram of normalized sheet resistance as a function of both temperature and the geometrical parameter L/d is given by the 3D color map of Figure 2c. In Figure 2d we visualize a projection of this phase diagram in the T vs. L/d plane, highlighting the correspondence between L/d and the *charge* $\langle \delta \rangle = 0.45 \times (1 - L/d)$.

We have used a least squares fitting algorithm extracting the parameters A , B , R_{0K} and T_K . The evolution of these parameters as a function of L/d are shown in Figure 3. In the sheet resistance measured at 150 K in all 18 measured samples with different L/d values, we observe an exponential increase for $L/d > 2/3$, indicating a metal insulator transition triggered by this geometrical conformational parameter. The evolutions of the fitting parameters A , B , $r_0 + R_{0K}$ T_K of Eq. 1 are shown in Figure 3b, Figure 3c, Figure 3d and Figure 3e. All parameters show a minimum at $L/d = 2/3$. Finally, in the scatter plot of T_K vs. R_{0K} , the positive correlation between these two parameters is made evident in Figure 3f.

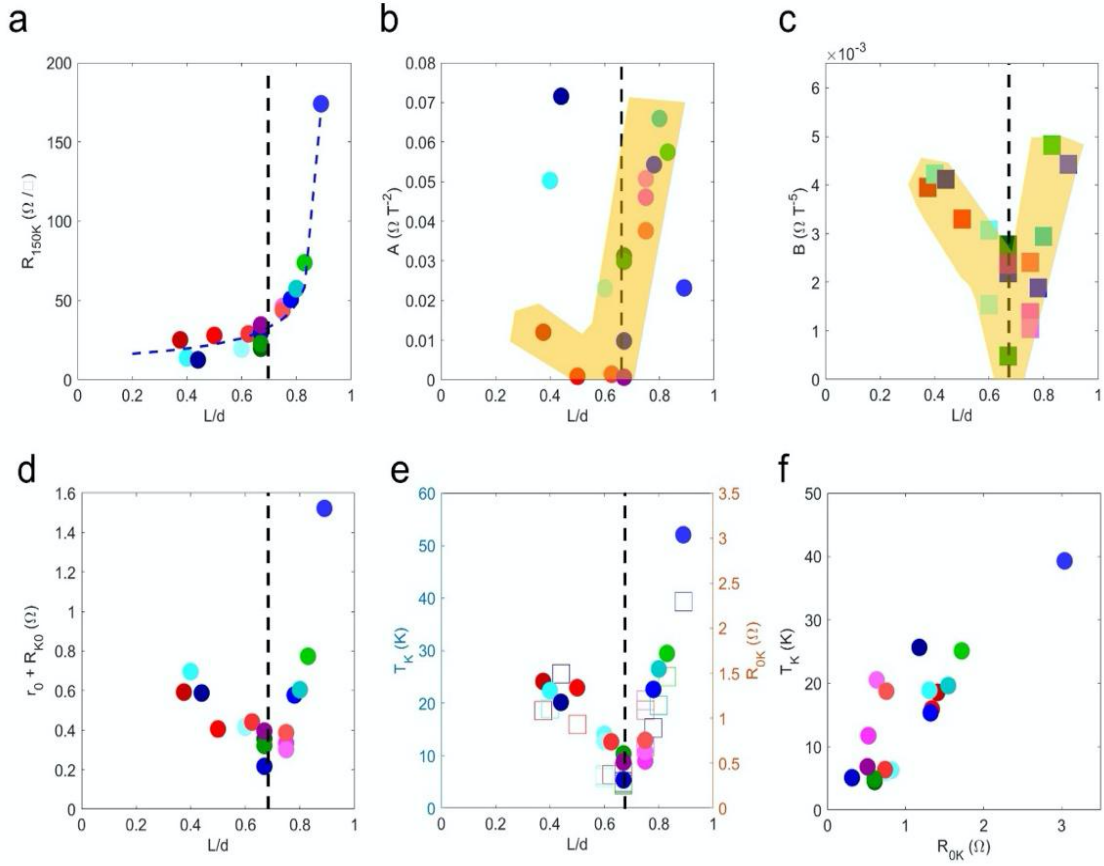


Figure 3. (a) Sheet resistance measured at 150 K in all 18 measured samples with different L/d values. We observe the exponential increase for $L/d > 0.667$. Evolution of fitting parameters (b) A , (c) B , (d) $r_0 + R_{0K}$ (e) T_K of Eq. 1. (f) Scatter plot of T_K versus R_{0K} showing the positive correlation between these two parameters.

Materials and Methods+

MBE Synthesis of Artificial High- T_c Superlattices: AHTS based on normal metal LSCO alternating with superconducting space charge layers in LCO thin layers have been synthesized via an ozone-assisted MBE method (DCA Instruments Oy) on LaSrAlO_4 (001) substrates (compressive strain for La_2CuO_4 on LaSrAlO_4 is +1.4%). The superlattice growth was controlled by the in-situ reflection high-energy electron diffraction (RHEED). This method is characterized by the sequence of deposition of single atomic layers and minimal kinetic energy of impinging atoms (about 0.1 eV). The substrate temperature, T_s , according to radiation pyrometer reading was 650°C , and the chamber pressure $p \approx 1.5 \times 10^{-5}$ Torr of mixed ozone, atomic and molecular oxygen. At the end of the procedure, the samples were cooled down in ozone to $T_s = 220^\circ\text{C}$. At this temperature the stoichiometric La_2CuO_4 layers [44] are free of oxygen interstitials dopants. Then the samples were cooled down in vacuum to avoid doping by oxygen interstitials."

Resistance measurements: The temperature dependence of resistance was determined in a four-point van der Pauw configuration with alternative DC current $\pm 10 \mu\text{A}$, in a temperature range from room

temperature to 4.2 K (liquid helium). The temperature dependent resistance was measured by using a motorized custom-made dipstick in a transport helium dewar with temperature rate <0.1 K/s.

Outline

It has been noticed by many authors that cuprate superconductors exhibiting high- T_c superconductivity show unconventional transport properties in the normal phase above the critical temperature, related with quantum tunneling characterized by T -linear resistivity, Planckian limit of the scattering rate assigned to quantum criticality, strong electronic correlation, coexistence of localized and itinerant states [32-43] in a homogeneous strange metal.

In this work we provide further experimental evidence that the Artificial High T_c Superlattices, made of modulation doped quantum wells formed by superconducting (S) layers of chemically stoichiometric Mott insulator La_2CuO_4 of thickness on the range of 2-3 nanometers intercalated by a normal metal (M), with the role of charge reservoir and a potential barrier of 500 meV [1] grab the key feature of natural chemical doped $\text{La}_{2-x}\text{Sr}_x\text{CuO}_4$.

We confirm that AHTS exhibit first (i) the *superconducting dome* of the critical temperature versus modulation doping and second (ii) T -linear Planckian sheet resistance around optimum modulation doping reported in reference [1]. These results falsify the decades old paradigm of a homogeneous strange metal near a quantum critical point for the interpretation of the phase diagrams of unconventional high- T_c superconductors. The present results support the physical paradigm describing unconventional high T_c cuprate perovskites characterized by intrinsic functional arrested chemical nanoscale phase separation observed by local and fast x-ray experimental probes [44-50] of the quantum complex matter landscape called “superstripes” [46] or “swiss cheese” [48] scenario where the electron gas is near a BEC-BCS crossover.

The key remarkable result, shedding further light on the mechanism of high T_c superconductivity, is that the proximity Kondo resistance competes with T -linear regime in the normal phase sheet resistance of doped cuprate AHTS. Where the Fano Feshbach resonance between two superconducting gaps determined by quantum size effects of the nanoscale units has been optimized by quantum design at the geometrical conformational parameter of the superlattice, $L/d=2/3$, at the top of the superconducting dome the Kondo temperature T_K reaches a minimum of the order of 4 Kelvin and the Kondo amplitude R_{0K} vanishes as shown in Fig.3. On both sides of the superconducting dome where the average doping is in the so-called overdoped $L/d < 2/3$ or underdoped regime $L/d > 2/3$ the Kondo temperature T_K increases and becomes higher than the superconducting critical temperature. These results are supported by the clear experimental anticorrelation between T_K and R_K . Finally it is remarkable that where the resonant quantum tunnelling driven by Fano-Feshbach

resonant is dominant also the residual $T=0\text{K}$ resistance, the amplitude of the electron-electron Fermi scattering term T^2 and the electron-phonon T^5 term vanish in the normal phase.

Authors

Email : antonio.bianconi@ricmass.eu, g.logvenov@fkf.mpg.de, sergio.caprara@uniroma1.it, antonio.valletta@cnr.it, gaetano.campi@ic.cnr.it

ORCID: Antonio Bianconi [0000-0001-9795-3913](https://orcid.org/0000-0001-9795-3913); Gennady Logvenov [0000-0003-1986-0249](https://orcid.org/0000-0003-1986-0249); Sergio Caprara [0000-0001-8041-3232](https://orcid.org/0000-0001-8041-3232) ; Antonio Valletta [0000-0002-3901-9230](https://orcid.org/0000-0002-3901-9230); Gaetano Campi [0000-0001-9845-9394](https://orcid.org/0000-0001-9845-9394)

Author Contributions:

Conceptualization, A.B. and G.L. and G.C.; methodology, G.L. and A.B.;

software, A.V., G.C. and A.B.; validation, G.L. and A.B.;

formal analysis, G.L., G.C. A.B.;

investigation, G.L., G.C. A.V. and A.B.;

sample synthesis, G.L.;

data curation, G.L., G.C. and A.B.;

writing original draft preparation A.B., G.C. , G.L. and S.C.;

writing review and editing, A.B., G.C.. S.C., ,G.L.;

All authors have read and agreed to the published version of the manuscript

Funding: This research received funding from Superstripes onlus.

Data Availability Statement: The data that support the findings of this study are available from the corresponding authors (A.B.. G.C.) upon reasonable request.

Conflicts of Interest: The authors declare no conflict of interest. The funders had no role in the design of the study; in the collection, analyses, or interpretation of data; in the writing of the manuscript; or in the decision to publish the results

References

1. Logvenov, G., Bonmassar, N., Christiani, G., Campi, G., Valletta, A., Bianconi, A. (2023). The superconducting dome in artificial high- T_c superlattices tuned at the Fano–Feshbach resonance by quantum design. *Condensed Matter*, 8(3), 78
2. Mazziotti, M. V., Valletta, A., Raimondi, R., Bianconi, A. (2021). Multigap superconductivity at an unconventional Lifshitz transition in a three-dimensional Rashba heterostructure at the atomic limit. *Physical Review B*, 103(2), 024523.
3. Mazziotti, M. V., Bianconi, A., Raimondi, R., Campi, G., Valletta, A. (2022). Spin–orbit coupling controlling the superconducting dome of artificial superlattices of quantum wells. *Journal of Applied Physics*, 132(19).
4. Mondal, D., Mahapatra, S. R., Derrico, A. M., Rai, R. K., Paudel, J. R., Schlueter, C., et al. (2023). Modulation-doping a correlated electron insulator. *Nature Communications*, 14(1), 6210. <https://doi.org/10.1038/s41467-023-41816-3>
5. Bianconi, A. (1994). On the possibility of new high T_c superconductors by producing metal heterostructures as in the cuprate perovskites. *Solid state communications*, 89(11), 933-936.
6. Bianconi, A., Valletta, A., Perali, A., Saini, N. L. (1998). Superconductivity of a striped phase at the atomic limit. *Physica C: Superconductivity*, 296(3-4), 269-280.
7. Bianconi, A. (2005). Feshbach shape resonance in multiband superconductivity in heterostructures. *Journal of Superconductivity*, 18, 625-636.

8. Bianconi, A., Innocenti, D., Valletta, A., Perali, A. (2014). Shape Resonances in superconducting gaps in a 2DEG at oxide-oxide interface. In *Journal of Physics: Conference Series* (Vol. 529, No. 1, p. 012007). IOP Publishing
9. Cariglia, M.; Vargas-Paredes, A.; Doria, M.M.; Bianconi, A.; Milošević, M.V.; Perali, A. (2016) Shape-resonant superconductivity in nanofilms: From weak to strong coupling. *J. Supercond. Nov. Magn.* 29, 3081–3086.
10. Salasnich, L.; Shanenko, A.A.; Vagov, A.; Aguiar, J.A.; Perali, A (2019). Screening of pair fluctuations in superconductors with coupled shallow and deep bands: A route to higher-temperature superconductivity. *Phys. Rev. B* 100, 064510.
11. Ochi, K.; Tajima, H.; Iida, K.; Aoki, H. Resonant pair-exchange scattering and BCS-BEC crossover in a system composed of dispersive and heavy incipient bands: A Feshbach analogy. *Phys. Rev. Res.* 2022, 4, 013032.e26. [CrossRef]
12. Valentinis, D.; Gariglio, S.; Fête, A.; Triscone, J.M.; Berthod, C.; Van Der Marel, D. Modulation of the superconducting critical temperature due to quantum confinement at the LaAlO₃/SrTiO₃ interface. *Phys. Rev. B* 2017, 96, 094518.
13. Barišić, N., Chan, M. K., Li, et al. (2013). Universal sheet resistance and revised phase diagram of the cuprate high-temperature superconductors. *Proceedings of the National Academy of Sciences*, 110(30), 12235-12240.
14. Kondo, J. (1964). Resistance minimum in dilute magnetic alloys. *Progress of Theoretical Physics*, 32(1), 37-49
15. Helmes, R. W., Costi, T. A., Rosch, A. (2008). Kondo proximity effect: How does a metal penetrate into a Mott insulator? *Physical Review Letters*, 101(6), 066802.
<https://doi.org/10.1103/PhysRevLett.101.066802>
16. Costi, T. A., Hewson, A. C., Zlatic, V. (1994). Transport coefficients of the Anderson model via the numerical renormalization group. *Journal of Physics: Condensed Matter*, 6(13), 2519–2558.
[doi:10.1088/0953-8984/6/13/013](https://doi.org/10.1088/0953-8984/6/13/013)
17. Yang, F., Wang, Z., Liu, Y., Yang, S., Yu, Z., An, Q., ... Liu, X. (2022). Engineered Kondo screening and nonzero Berry phase in SrTiO₃/LaTiO₃/SrTiO₃ heterostructures. *Physical Review B*, 106(16), 165421. [Doi: 10.1103/PhysRevB.106.165421](https://doi.org/10.1103/PhysRevB.106.165421) <https://doi.org/10.1103/PhysRevB.106.165421>
18. Zhuravlev, A. K., Anokhin, A. O., Irkhin, V. Y. (2018). One- and two-channel Kondo model with logarithmic Van Hove singularity: A numerical renormalization group solution. *Physics Letters A*, 382(7), 528–533. [doi:10.1016/j.physleta.2017.12](https://doi.org/10.1016/j.physleta.2017.12).
19. Kourris, C., Vojta, M. (2023). Kondo screening and coherence in kagome local-moment metals: Energy scales of in the presence of flat bands. *Physical Review B*, 108(23), 235106.
20. Kar, I., Ghosh, S., Gupta, S., Chakraborty, S., Thirupathiah, S. (2024). Comparative study of Kondo effect in vanadium dichalcogenides VX₂ (X= Se Te). *Physica B: Condensed Matter*, 674, 415532.
21. Hien-Hoang, V., Chung, N.K., Kim, H.J. (2021) Electrical transport properties and Kondo effect in La_{1-x}Pr_xNiO_{3-δ} thin films. *Sci Rep* 11, 5391 <https://doi.org/10.1038/s41598-021-84736-2>
22. Shimizu, H., Oka, D., Kaminaga, K., Saito, D., Yamamoto, T., Abe, N., ... Fukumura, T. (2022). Rocksalt-type PrO epitaxial thin film as a weak ferromagnetic Kondo lattice. *Physical Review B*, 105(1), 014442. <https://doi.org/10.1103/PhysRevB.105.014442>
23. Shankar, A. S., Oriekhov, D. O., Mitchell, A. K., Fritz, L. (2023). Kondo effect in twisted bilayer graphene. *Physical Review B*, 107(24), 245102.
24. Miura, N., Nakagawa, H., Sekitani, T., Naito, M., Sato, H., Enomoto, Y. (2002). *High-magnetic-field study of high-Tc cuprates*. *Physica B: Condensed Matter*, 319(1-4), 310–320. [doi:10.1016/s0921-4526\(02\)01134-1](https://doi.org/10.1016/s0921-4526(02)01134-1)
25. Sekitani, T., Naito, M., Miura, N. (2003). Kondo effect in underdoped n-type superconductors. *Physical Review B*, 67(17). [doi:10.1103/physrevb.67.174503](https://doi.org/10.1103/physrevb.67.174503)
26. Yin, H. T., Liu, X. J., Feng, L. F., Lü, T. Q., Li, H. (2010). Spin-dependent Kondo effect induced by Rashba spin-orbit interaction in parallel coupled double quantum dots. *Physics Letters A*, 374(28), 2865-2873
27. Bulka, B. R., Stefański, P., Tagliacozzo, A. (2005). Interplay of Kondo and Fano resonance in electronic transport in nanostructures. *Acta Physica Polonica A*, 108(4), 555-569.
28. Fang, T. F., Luo, H. G. (2010). Tuning the Kondo and Fano effects in double quantum dots. *Physical Review B*, 81(11), 113402.
29. Stefański, P. (2010). Interplay between quantum interference and electron interactions in a Rashba system. *Journal of Physics: Condensed Matter*, 22(50), 505303.

30. Misawa, T., Nomura, Y., Biermann, S., Imada, M. (2016). Self-optimized superconductivity attainable by interlayer phase separation at cuprate interfaces. *Science advances*, 2(7), e1600664
31. Tadano, T., Nomura, Y., Imada, M. (2019). Ab initio derivation of an effective Hamiltonian for the $\text{La}_2\text{CuO}_4/\text{La}_{1.55}\text{Sr}_{0.45}\text{CuO}_4$ heterostructure. *Physical Review B*, 99(15), 155148.
32. Phillips, J. C. (1989). Reconciliation of normal-state and superconductive specific-heat, optical, tunneling, and transport data on Y-Ba-Cu-O. *Physical Review B*, 40(10), 7348–7349. doi:10.1103/physrevb.40.7348
33. Varma, C. M., Littlewood, P. B., Schmitt-Rink, S., Abrahams, E., Ruckenstein, A. E. (1989). Phenomenology of the normal state of Cu-O high-temperature superconductors. *Physical Review Letters*, 63(18), 1996.
34. Martin, S., Fiory, A. T., Fleming, R. M., Schneemeyer, L. F., Waszczak, J. V. (1990). Normal-state transport properties of $\text{Bi}_{2+x}\text{Sr}_{2-y}\text{CuO}_{6+\delta}$ crystals. *Physical Review B*, 41(1), 846–849. doi:10.1103/physrevb.41.846
35. Zaanen, J. Why the temperature is high. *Nature* **430**, 512–513 (2004). <https://doi.org/10.1038/430512>
36. Cooper, R. A., Wang, Y., Vignolle, B., et al. (2009). Anomalous criticality in the electrical resistivity of $\text{La}_{2-x}\text{Sr}_x\text{CuO}_4$. *Science*, 323(5914), 603-607
37. Bruin, J. A. N., Sakai, H., Perry, R. S., Mackenzie, A. P. (2013). Similarity of scattering rates in metals showing T-linear resistivity. *Science*, 339(6121), 804–807. doi:10.1126/science.1227612
38. Haldane, F. D. M. (2018). Fermi-surface geometry and "Planckian dissipation". *arXiv preprint arXiv:1811.12120*.
39. Shaginyan, V. R., Amusia, M. Y., Msezane, A. Z., Stephanovich, V. A., Japaridze, G. S., Artamonov, S. A. (2019). Fermion condensation, T-linear resistivity, and Planckian limit. *JETP Letters*, 110, 290-295.
40. Amusia, M., Shaginyan, V. (2020). Quantum Criticality, T-linear Resistivity, and Planckian Limit. In: Strongly Correlated Fermi Systems. Springer Tracts in Modern Physics, vol 283. Springer, Cham. doi: 10.1007/978-3-030-50359-8_22.
41. Patel, A. A., Sachdev, S. (2019). Theory of a Planckian metal. *Physical review letters*, 123(6), 066601.
42. Legros, A., Benhabib, S., Tabis, W., Laliberté, F., Dion, M., Lizaire, M., ... & Proust, C. (2019). Universal T-linear resistivity and Planckian dissipation in overdoped cuprates. *Nature Physics*, 15(2), 142-147.
43. Balm, F., Chagnet, N., Arend, S., Aretz, J., Grosvenor, K., Janse, M., Zaanen, J. (2023). T-linear resistivity, optical conductivity, and Planckian transport for a holographic local quantum critical metal in a periodic potential. *Physical Review B*, 108(12), 125145.
44. Fratini, M., Poccia, N., Ricci, A., Campi, G., et al. (2010). Scale-free structural organization of oxygen interstitials in $\text{La}_2\text{CuO}_{4+y}$. *Nature*, 466(7308), 841-844.
45. Campi, G., Bianconi, A., Poccia, N., et al. (2015). Inhomogeneity of charge-density-wave order and quenched disorder in a high- T_c superconductor. *Nature*, 525(7569), 359-362
46. Bianconi, A. (2013). Shape resonances in superstripes. *Nature Physics*, 9(9), 536-537.
47. Jarlborg, T., Bianconi, A. (2013). Fermi surface reconstruction of superoxygenated La_2CuO_4 superconductors with ordered oxygen interstitials. *Physical Review B—Condensed Matter and Materials Physics*, 87(5), 054514.
48. Uemura, Y. J. (1997). Bose-Einstein to BCS crossover picture for high- T_c cuprates. *Physica C: Superconductivity*, 282, 194-197.
49. Li, Y., Sapkota, A., Lozano, P. M., Du, et al. (2022). Strongly overdoped $\text{La}_{2-x}\text{Sr}_x\text{CuO}_4$: Evidence for Josephson-coupled grains of strongly correlated superconductor. *Physical Review B*, 106(22), 224515.
50. Giraldo-Gallo, P., Zhang, Y., Parra, C., Manoharan, H. C., Beasley, M. R., Geballe, T. H., ... & Fisher, I. R. (2015). Stripe-like nanoscale structural phase separation in superconducting $\text{BaPb}_{1-x}\text{Bi}_x\text{O}_3$. *Nature communications*, 6(1), 8231.